ELSEVIER

Journal of Power Sources 63 (1996) 115–120

JOURNAL OF POWER SOURCES

Gas-flow uniformity and cell performance in a molten carbonate fuel cell stack

Haruhiko Hirata, Michio Hori

Research and Development Center, Toshiba Corporation, 4-1, Ukishima-cho, Kawasaki-ku, Kawasaki 210, Japan

Received 19 June 1996; accepted 29 July 1996

Abstract

An examination is made of the relationships between the gas-flow uniformity in the planar direction, the gas-flow uniformity in the stacking direction, and the cell performance in a co-flow type molten carbonate fuel cell stack. A simulation code that accounts for the effects of electrochemical reactions, heat transfer, and gas flow is used to calculate the cell performance (i.e. cell temperature, current density and cell voltage) for various gas-flow uniformity levels in both the planar and the stacking directions. A comparison is made of the effects of the two kinds of gas flow uniformity on the cell performance.

Keywords: Molten carbonate fue cells; Simulation; Gas flow; Cell performance

1. Introduction

In recent years, molten carbonate fuel cells (MCFCs) have attracted strong interest due to expectations that they will serve as highly efficient, low-pollution power sources. Various types of cell stack structure have been examined with a view to realizing commercial plants. Of these structures, a stack using a co-flow configuration, in which both fuel gas and oxidant gas are led in the same direction along a unit cell, has been recognized as one of the practical structures to realize uniform cell reaction and cell temperature. Due to a lack of detailed information on the relation between gas-flow uniformity and cell performance, however, a major effort has been devoted to improving the uniformity of the gas-flow in order to increase cell performance.

A stack with plate heat-exchanger type separators is shown schematically in Fig. 1. The gas flows in the separators are in a co-flow configuration, while the manifold structures are in an internal manifold configuration. In the stack, the edge and manifold seal portions are separated, and a wet gas seal is used for the edge and a connected solid parts gas seal for the manifold. Therefore, at the manifold portions, in which a large amount of gas flows, a tight gas seal is maintained by the connected seal configuration. The edge and manifold portions are also designed to be flexible so that they follow the creep deformation of the active portions, and therefore a good electrical contact at the active portion and a tight gas seal at the edge and manifold are reliably maintained.

PII S0378-7753(96)02459-7

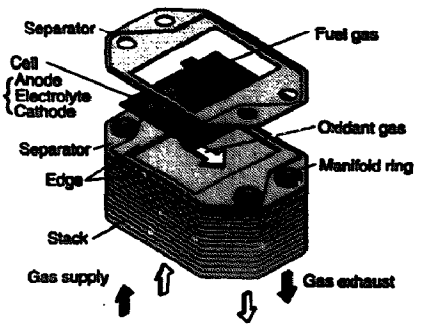

Fig. 1. Plate heat-exchanger type stack.

On the other hand, careful design is required to realize uniform gas flow in the planar direction (i.e. the direction along the cell plane) of the stack, due to the divergent and convergent gas channels, as well as in the stacking direction, due to the small section size of the manifold compared with the outer manifold configuration. Therefore, to realize a rational stack design, it is necessary to understand the relation between gas-flow uniformity and cell performance.

In this study, the relationships between the gas-flow uniformity in the planar direction, the gas-flow uniformity in the stacking direction, and the cell performance are examined using a specially-devised simulation model.

2. Method of analysis

The operating principle of an MCFC is shown in Fig. 2. The electricity is generated in the active portion which con-

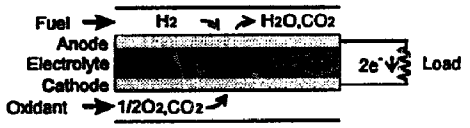

Fig. 2. Principle of the MCFC.

sists of the electrolyte, the anode, and the cathode. The electrolyte consists of molten carbonate which is contained in a porous matrix. A fuel gas that contains H_2 is fed to the anode, and an oxidant gas that contains O_2 and CO_2 is fed to the cathode. The following electrode reactions take place at each electrode:

(i) cathode

$$1/2O_2 + CO_2 + 2e^- \rightarrow CO_3^{2-} \quad (1)$$

(ii) anode

$$H_2 + CO_3^{2-} \rightarrow H_2O + CO_2 + 2e^- \quad (2)$$

These reactions are exothermic overall, and transfer of CO_3^{2-} ions in the electrolyte drives electron flow in the load.

At the anode, the following shift reaction is also assumed to be in the equilibrium state

$$H_2 + CO_2 \rightleftharpoons H_2O + CO \quad (3)$$

The analysis model consists of a unit cell (i.e. electrolyte, anode, and cathode), two separators, a fuel gas, and an oxidant gas; it is shown schematically in Fig. 3. The two separators are assumed to have the same temperature distribution when modelling a tall stack composed of many cells.

The following mass balances between molar flux n_i of reactive gases and the current density i are satisfied:

(i) cathode side

$$div n_{O_2} = -i/4Fh_c \quad (4a)$$

$$div n_{CO_2} = -i/2Fh_c \quad (4b)$$

(ii) anode side

$$div n_{H_2} = -i/2Fh_a \quad (5a)$$

$$div n_{CO_2} = i/2Fh_a \quad (5b)$$

$$div n_{H_2O} = i/2Fh_a \quad (5c)$$

The open-circuit voltage, E, is determined from the standard electromotive force, E_0, of the electrode reaction, which is shown as Eqs. (1) and (2), and the gas composition using the Nernst equation

$$E = E_0 + \frac{RT}{2F} \ln \frac{(P_{H_2})_a (P_{CO_2} P_{O_2}^{1/2})_c}{(P_{H_2O} P_{CO_2})_a} \quad (6)$$

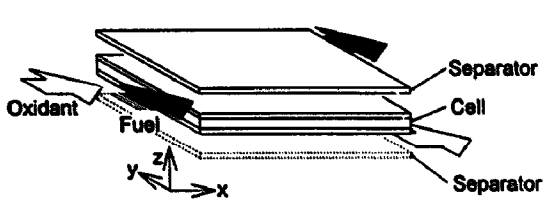

Fig. 3. Analysis of model of a unit cell of the MCFC.

The cell voltage, V, is determined by E, i, and effective resistance R_{eff} which contains the anode and cathode overpotentials and ohmic loss

$$V = E - R_{eff} i \quad (7)$$

R_{eff} is assumed, as shown in Table 1, based on the experimental results for small unit cells.

The heat generation, q_e, by the electrode reaction is derived as follows

$$q_e = -\Delta H_e (i/2F) - Vi \quad (8)$$

where ΔH_e is the enthalpy change of the electrode reaction. The heat generation (or heat consumption) q_s due to the shift reaction is derived from the enthalpy change of the shift reaction ΔH_s and the molar flow rate change Δn_{CO} of CO on the unit anode area

$$q_s = \Delta H_s \Delta n_{CO} \quad (9)$$

The heat generation and heat consumption were also assumed to occur in the cell.

For the heat transfer, the cell and separator were assumed to have uniform temperature in each thickness, and the mean temperature in each thickness were treated for the fuel gas and oxidant gas. For the cell, thermal conductivity in the planar direction, convective heat transfer between the cell and the fuel and oxidant gases, and radiative heat transfer between the cell and the separator were considered. The energy balance for the cell is derived as follows

$$-\lambda_c t_c \nabla^2 T_c = \alpha_F (T_F - T_C) + \alpha_O (T_O - T_C) + \sum_{n=1}^{2} \sigma \epsilon_n F_n (T_{Sn}^4 - T_C^4) + q_e + q_s \quad (10)$$

where T_C is cell temperature, T_F and T_O are the fuel and the oxidant gas temperature, n indicates the anode-side separator when n equals 1, and the cathode-side separator when equals 2, respectively; T_{S1} and T_{S2} are the anode-side and the cathode-side separator temperature; the anode and oxidant gas channel heat-transfer coefficients α_F and α_O were derived from the Nusselt number for a parallel-plate channel. The geometrical factors F_n were assumed to be 1 (in the case where the cell and the separator elements were fully over-

Table 1
Principal analysis conditions

Cell size	1 m × 1 m
Gas channel height, h_a, h_c	1.4×10^{-3} m
Inlet gas composition	Fuel H_2:CO_2:H_2O = 70:18:12
	Oxidant O_2:CO_2:N_2 = 14:30:56
Inlet gas temperature	923 K
Pressure	0.1 MPa
Current density	1500 A m^{-2}
Effective resistance, R_{eff}	$1.88 \times 10^{-7} \exp(4.85 \times 10^4/RT)$ Ω m^{-2}
Thermal conductivity	λ_C = 7.07 W m^{-1} K^{-1},
	λ_S = 22.9 W m^{-1} K^{-1}
Gas channel Nusselt number	8.23
Emissivity, ϵ_n	0.48

lapped) or 0 (in the case where the cell and separator elements were not overlapped). A similar energy balance for the separator is obtained by simply omitting q_e and q_s from Eq. (10).

For the fuel gas, enthalpy transfer by gas flow, convective heat transfer between the fuel gas and the cell and separator, and enthalpy transfer by CO_3^{2-} ion transfer were considered. The energy balance for the fuel gas is derived as follows

$$h_a div(c_{pF}T_F n_F) = \alpha_F(T_C - T_F) + \alpha_F(T_S - T_F) + (i/2F)c_{pCO_3}T_O \quad (11)$$

where n_F is the molar flux of fuel gas, and c_{pCO_3} is the specific heat of the composite gas which consists of O_2 and CO_2 at a ratio of 1:2. The similar energy balance for the oxidant gas is derived by merely inverting the sign of the third term in Eq. (11).

For the gas flow, considering O_2 and CO_2 transfer by the electrode reaction, mass balance for the fuel gas is

$$div(\rho_F u_F) = (i/2Fh_a)(M_{O_2}/2 + M_{CO_2}) \quad (12)$$

where u_F is the fuel gas mean velocity in the thickness; ρ_F is the fuel gas density; M_{O_2} and M_{CO_2} are the mol. wt. of O_2 and CO_2, respectively. The similar mass balance for the oxidant gas is derived by inverting the sign of the right-hand term. Assuming two-dimensional Poiseuille flows in the x- and y-directions, the momentum balances for the fuel gas are:

$$u_{Fx} = (-dp_F/dx)(h_a^2/12\mu_F) \quad (13)$$

$$u_{Fy} = (-dp_F/dy)(h_a^2/12\mu_F) \quad (14)$$

where p_F is the static pressure of the fuel gas; u_{Fx} and u_{Fy} are the mean velocity components in the x- and y-directions, respectively. Similar relations between the velocities and static pressure are derived for the oxidant gas.

To solve the coupling phenomena in the fuel cell, that are expressed in Eqs. (1) to (14), a modelling by the nodal network method was adopted. The cell was divided into elements with uniform temperatures, current densities, and open-circuit voltages. The separator was divided into elements with uniform temperatures. The fuel gas and oxidant gas were divided into elements with uniform temperatures, partial pressures of chemical species, and static pressures. Each element was connected by elements with certain thermal conductances, and the fuel and oxidant gas elements were also connected by elements with specific flow resistance. The calculations for the electrochemical reactions and the matrix solutions for the temperature and static pressure were performed iteratively and, as the result of convergence, steady-state solutions that contain non-linear effects for the phenomena were obtained.

3. Analysis conditions

For the evaluation of the effect of the planar direction flow uniformity on the cell performance, the velocity distributions of the fuel and oxidant gases at the inlet and outlet of the active portion were assumed to have various uniformity. Each normalized velocity distribution of fuel and oxidant gases for the flow deviations of 0, 5, 10, 20, 30, 40 and 50% are shown in Fig. 4. Here, the flow deviations are defined as the normalized standard deviations of the gas velocity distributions. The velocity distribution patterns are decided by assuming a plate heat-exchanger type fuel-cell stack that has an inlet manifold and an outlet manifold placed on the opposite sides of the neutral axis relative to one another, as shown in Fig. 1.

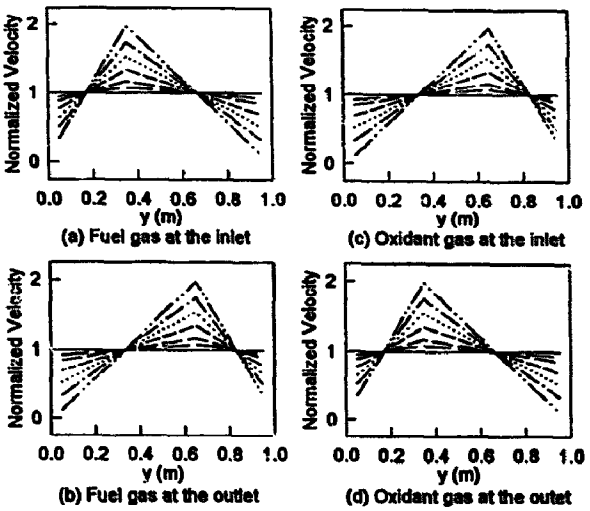

Fig. 4. Fuel and oxidant gas velocity distributions at the inlet and outlet of active area for various flow deviations: (———) 0%; (— —) 5%; (– – –) 10%; (– · – ·) 20%; (· · · · ·) 30%; (– · · –) 40%, and (– · · · –) 50%.

The relations between gas utilizations and cell performances were also examined to evaluate the effect of stacking direction flow uniformity on the cell performance. The gas utilizations are defined as the ratios of utilized H_2 and O_2 to those at the inlet; when the gas flow rates at the inlet are increased, the utilizations are decreased proportionally. Here, the gas utilizations indicate gas flow rates for a cell which is a part of the stacked cells, and the changes in the utilizations indicate the uniformity change of the gas flow in the stacking direction. The fuel and oxidant gas utilizations are assumed to be 80 and 10%, 80 and 40%, 50 and 10%, and 50 and 40%, respectively. The other principal analysis conditions are shown in Table 1.

The cell performances (i.e. cell voltage, current-density distribution, and cell-temperature distribution) under these flow uniformity conditions are evaluated.

4. Results and discussion

The fuel and oxidant gas velocities, current density, and cell temperature were recorded for typical gas utilization when the fuel utilization U_F was 80% and oxidant utilization U_O was 10%. The results for flow deviations of 0, 20 and 50% are shown in Figs. 5–7, respectively. As the flow deviation increased, the patterns of current-density distributions and cell-temperature distributions became more complex in

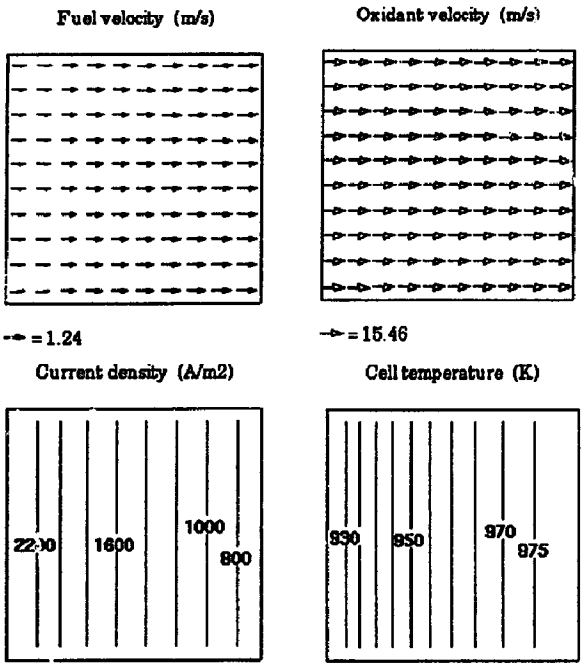

Fig. 5. Fuel and oxidant gas velocities, current density, and cell temperature for 0% flow deviation, $U_F = 80\%$, and $U_O = 10\%$.

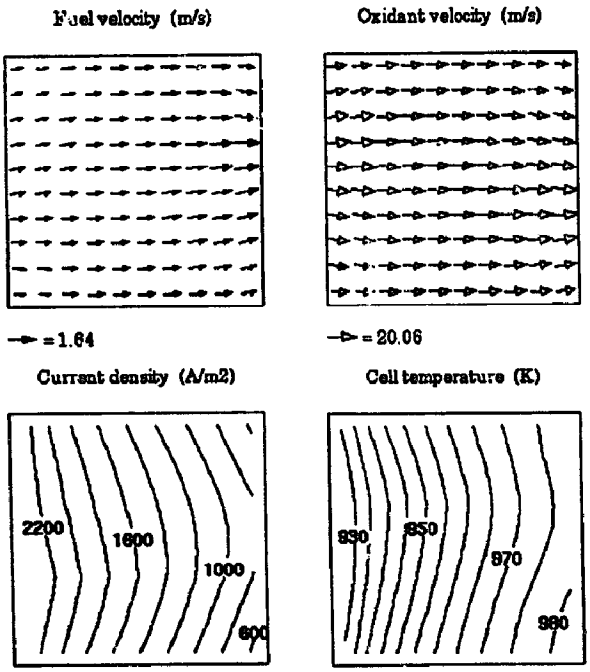

Fig. 6. Fuel and oxidant gas velocities, current density, and cell temperature for 20% flow deviation, $U_F = 80\%$, and $U_O = 10\%$.

accordance with the fuel and oxidant velocity distributions. The current-density distribution is strongly influenced by the fuel gas velocity distribution, because the current density is mainly determined by the H_2 concentration of the fuel gas in the case of high fuel utilization. The cell-temperature distribution is strongly influenced by the oxidant gas velocity distribution, because the cell temperature is mainly determined

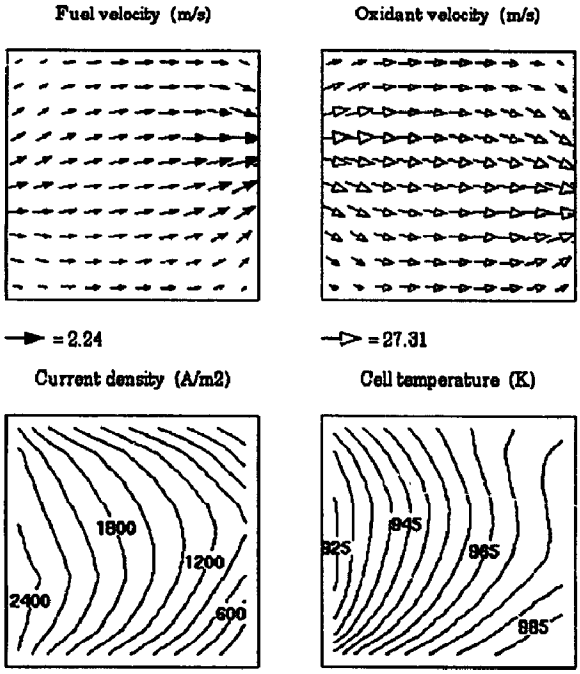

Fig. 7. Fuel and oxidant gas velocities, current density, and cell temperature for 50% flow deviation, $U_F = 80\%$, and $U_O = 10\%$.

by the enthalpy transfer by the oxidant gas in the case of low oxidant utilization.

The patterns of the fuel and oxidant velocity distribution, the current-density distribution, and the cell temperature distribution for the other gas utilization cases were similar to the patterns for the above case of U_F is 80% and U_O is 10%, if the flow deviations were the same. By contrast, the current-density range and maximum cell temperature were different for each gas utilization condition.

As described above, it becomes possible to calculate the effects of gas flow patterns on the cell performance by using the code. For the plate heat-exchanger type stack in which the outlet gas velocity distribution differs from the inlet gas velocity distribution, as shown in Fig. 7, it is also possible to evaluate these effects by assuming two-dimensional gas flow along the active portion.

The effects of the flow deviation on the cell performance are given in Fig. 8. The relationships between normalized current density ranges and flow deviations for each fuel and oxidant utilization are presented in Fig. 8(a). The relationships between the normalized maximum cell temperatures and flow deviations for each fuel and oxidant utilization are given in Fig. 8(b). Finally, the relationships between the normalized cell voltage and flow deviations for each fuel and oxidant utilization are shown in Fig. 8(c). Here, every flow deviation was defined on the inlet of the active portion, and the values were normalized on the basis of the values for 0% flow deviation for each utilization.

The current-density range was defined as the difference between the maximum and minimum current density in the cell, and represents the uniformity of the electrode reaction

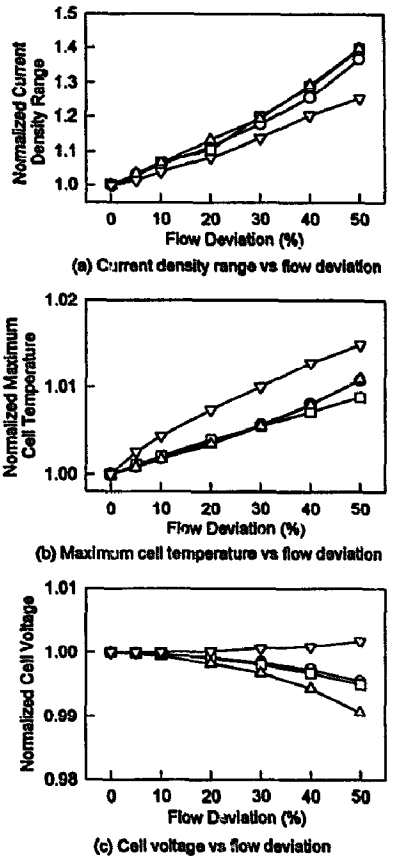

Fig. 8. Effect of the flow deviation on the ycell performance: (○) $U_F = 50\%$, $U_O = 10\%$; (□) $U_F = 50\%$, $U_O = 40\%$; (△) $U_F = 80\%$, $U_O = 10\%$; (▽) $U_F = 80\%$, $U_O = 40\%$.

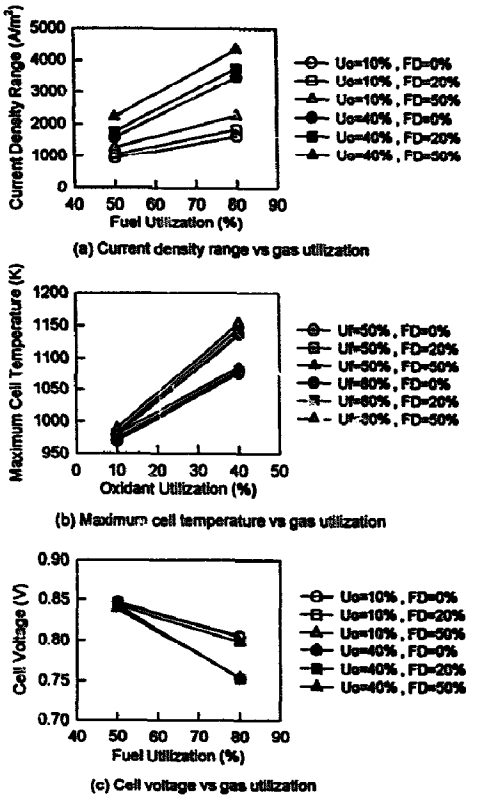

Fig. 9. Effect of the flow deviation and gas utilization on the cell performance.

at the active portion. For the purpose of operating every cell portion under the designed load condition and avoiding cell life shortening caused by overload, it is desirable to decrease the current-density range. As the flow deviation increased from zero to 50%, the current-density range increased by almost 40%. In order to avoid shortening of cell life by high temperature, it is desirable to decrease the maximum cell temperature. As the flow deviation increased from zero to 50%, the maximum cell temperature increased about 1%. To increase the electrical power, it is desirable to increase the cell voltage. As the flow deviation increased from zero to 50%, the cell voltage decreased by almost 1%.

The decrease of flow uniformity led to a decline in cell performance. Except for the current-density range, however, the effect of the flow deviation on the cell performance is slight. In these results, the case of $U_F = 80\%$ and $U_O = 40\%$ was disassociated from the others, because of the cell voltage increase that occurred due to the cell temperature rise caused by the high utilizations of the fuel and oxidant.

In a cell of a plate heat-exchanger type stack, flow deviation has been estimated as 25% at the most [1]. Therefore, decreases in cell performance for the plate heat-exchanger type stack are estimated as only 15% in current density, 0.5% in maximum cell temperature, and 0.2% in cell voltage. Here, the decline ratios are based on cell performance for 0% flow deviation in which cell performance is the best.

The effects of the gas utilization and flow deviation on the cell performance are illustrated in Fig. 9. The relationship between current-density range and fuel utilization for each oxidant utilization and flow deviation (FD) is given in Fig. 9(a), the relation between maximum cell temperature and oxidant utilization for each fuel utilization and FD in Fig. 9(b), and the relation between cell voltage and fuel utilization for each oxidant utilization and FD in Fig. 9(c). As the fuel utilization increased from 50 to 80%, the current-density range increases about 75% for the oxidant utilization $U_0 = 10\%$, and 95% to 117% for $U_O = 40\%$. As the oxidant utilization increases from 10 to 40%, the maximum cell temperature increases about 11% for the fuel utilization $U_F = 50\%$, and about 17% for $U_F = 80\%$. Finally, as the fuel utilization increases from 50 to 80%, the cell voltage decreases 5% for $U_O = 10\%$, and 11% for $U_O = 40\%$. Thus, increase in fuel and oxidant utilization leads to a decline in cell performance. On the other hand, as described above, the effects of a change in flow deviation on the cell performance were only 40% for current density, 1% for maximum cell temperature, and 1% for cell voltage, respectively.

Clearly the decline in cell performance caused by a change in gas FD is about a half of that for the current density and about a tenth of that for the maximum cell temperature and cell voltage caused by changes in fuel and oxidant gas utilization. The fuel and oxidant utilization changes from the

designed value occur when there is non-uniform gas feeding to each stacked cell. In other words, the decline in cell performance caused by the change of flow uniformity in the planar direction is much less than that caused by the change of the flow uniformity in the stacking direction.

In actual co-flow internal manifold type MCFC stacks, the flow uniformity in the planar direction can be improved by a rational design in the separator gas channel. The flow uniformity in the stacking direction can be improved by a rational design in the manifold. In these designs, it is more important for the cell performance to keep the flow uniformity in the stacking direction than in the planar direction.

5. Conclusions

The relations among the gas flow uniformity in the planar direction, the gas flow uniformity in the stacking direction, and the cell performance in a co-flow internal manifold type MCFC stack have been evaluated by using a simulation code that accounts for the effects of electrochemical reactions, heat transfer, and gas flow. In the stack, the effect on the cell performance (i.e. current-density range, maximum cell temperature, and cell voltage) due to lack of gas-flow uniformity in the planar direction is not critical. By contrast, the effect on cell performance of gas-flow uniformity in the stacking direction is about 2 to 10 times greater. Therefore, it is important to achieve gas-flow uniformity in the stacking direction in order to attain the designed cell performance.

6. List of symbols

c_p specific heat, J mol^{-1} K^{-1}
F Faraday constant, 96 487 A s mol^{-1}
F_n geometrical factor
h channel height, m
i current density, A m^{-2}
n molar flux, mol s^{-1} m^{-2}
n_j molar flux component for the j-direction
P partial pressure, Pa
R universal gas constant, 8.3143 J mol^{-1} K^{-1}
t cell or separator thickness, m

Greek letters

α heat-transfer coefficient, W m^{-2} K^{-1}
ϵ_n emissivity between two surfaces
λ heat conductivity, W m^{-1} K^{-1}
μ viscosity, Pa s
σ Stefan–Boltzmann constant, 5.6687×10^{8} W m^{-2} K^{-4}

Operator symbols

$div\, n$ $\partial n_x/\partial x + \partial n_y/\partial y$
∇^2 $\partial^2/\partial x^2 + \partial^2/\partial y^2$

Subscripts

a anode
c cathode
C cell
S separator
F fuel
O oxidant

References

[1] H. Hirata and M. Hori, *Proc. 34th Battery Symposium in Japan, Hiroshima, Japan, 1993*, p. 127.